Joint Optimization of Power Allocation and Beamforming for UAV-RIS Communication System

Xinying Guo, Longfei Liu, Jiankang Zhang, *Senior Member, IEEE*, Sheng Chen, *Life Fellow, IEEE*

***Abstract*—This paper considers the communication system assisted by a fixed-trajectory unmanned aerial vehicle (UAV), which is equipped with a reconfigurable intelligent surface (RIS). For this UAV-RIS assisted system, we jointly optimize the power allocation and active beamforming at the base station (BS) and the passive beamforming at the RIS, by a novel phase block coordinate descent algorithm framework aimed at maximizing the system sum-rate. Specifically, the joint optimization problem is decomposed into two phases, and we propose two optimization algorithms: one for BS power allocation using fractional programming (FP) and the other for jointly optimizing active and passive beamforming using FP-manifold, which alternately optimize two phases. Simulation results not only highlight the rapid convergence and evident superiority of our proposed framework but also reveal that the optimal UAV-RIS placement is related to the flight height.**

***Index Terms*—Beamforming, power allocation, reconfigurable intelligent surface, unmanned aerial vehicle.**

I. Introduction

Reconfigurable intelligent surface (RIS) with programmable electromagnetic properties is capable of appropriately adjusting the amplitude, phase, polarization and other characteristics of incident electromagnetic waves to improve wireless channel conditions and signal transmission efficiency [1]. Integrating RIS with unmanned aerial vehicle (UAV) as relays leverages UAVs' high mobility for flexible RIS deployment and utilizes RIS's passive elements for signal reflection and regulation without additional power supply [2], [3]. Compared to traditional UAV relays and stationary RIS-assisted communication systems, UAV integrated RIS (UAV-RIS) systems offer lower power consumption and higher spectral efficiency [4].

Addressing optimization challenges in RIS-assisted wireless systems requires careful consideration of a wide array of variables, which can either enhance or impede the system's spectral and energy efficiency. The work [5] introduced an alternating optimization (AO) framework with semi-definite relaxation (SDR) to jointly optimize active and passive beamforming, focusing on minimizing the base station (BS) transmission power. In [6], RIS passive beamforming was optimized using a manifold optimization algorithm, which demonstrates superior performance compared to that of the SDR method. The study [7] proposed a method combining the block coordinate descent (BCD) algorithm with successive convex approximation (SCA) for jointly optimizing active and passive beamforming, where SCA is less complex than manifold optimization algorithms. The work [8] maximized the sum rate of an aerial RIS-aided multiple-input multiple-output ground communication system, by using the BCD framework to jointly optimize active and passive beamforming and aerial RIS deployment. In [9], the system weighted sum-rate was maximized using a manifold optimization algorithm under the AO framework for the joint optimization of active and passive beamforming. Additionally, geometric programming (GP) was utilized in [9] for BS power allocation. These optimization algorithms studied in the literature however were mostly based on the AO and BCD frameworks, which may lead to high computational complexity.

This paper presents a novel phase BCD (PBCD) framework tailored to address the multi-variable joint optimization problem. Unlike traditional AO and BCD frameworks, which typically update each variable only once per iteration before alternating to the next variable, the PBCD framework segments the optimization problem into multiple phases based on the characteristics of the variables. In each phase, it updates a set of variables iteratively until convergence is achieved before proceeding to the next phase. In this paper, the PBCD framework is specifically employed to maximize the system sum-rate by strategically breaking down the optimization problem into two distinct phases. Building upon the PBCD framework, we propose a power allocation algorithm leveraging fractional programming (FP) and an AO algorithm for the joint optimization of active and passive beamforming utilizing the FP-manifold approach. Simulation results showcase our algorithms' robust convergence and lower computational complexity, compared with existing schemes. Moreover, the results reveal that the optimal location for the UAV-RIS is influenced by the UAV-RIS's height.

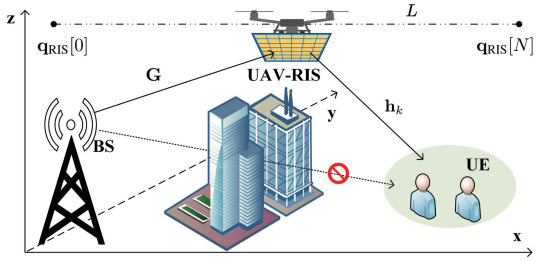

Fig. 1. Illustration of UAV-RIS assisted communication system.

II. Optimization Problem Formulation

A. System Model

Fig. 1 illustrates the UAV-RIS assisted communication system considered, where the BS employs M uniform-linear-

This work was supported by the National Natural Science Foundation of China (Grants 61901159) and the Cultivation Programme for Young Backbone Teachers in Henan University of Technology (Grants 21420104).

X. Guo (guoxinying@haut.edu.cn) and L. Liu (liulf@stu.haut.edu.cn) are with Key Laboratory of Grain Information Processing and Control (Henan University of Technology), Ministry of Education; and also with College of Information Science and Engineering, Henan University of Technology, Zhengzhou 450001, China.

J. Zhang (jzhang3@bournemouth.ac.uk) is with Department of Computing & Informatics, Bournemouth University, BH12 5BB, UK.

S. Chen (sqc@ecs.soton.ac.uk) is with School of Electronics and Computer Science, University of Southampton, Southampton SO17 1BJ, UK.

array antennas and the UAV integrates a RIS containing $R = R_x \times R_y$ uniform planar array elements to serve K single-antenna user equipment (UEs). We assume that the UAV-RIS flies from the start point to the end point along a straight line L at height H and speed V_{avg}. The flight period T is divided into N time slots, each of duration ∇t. The horizontal coordinate of the UAV-RIS in the n-th time slot is $\mathbf{q}_{\text{RIS}}[n] = \big[x_{\text{RIS}}[n], y_{\text{RIS}}[n]\big]$, $n \in \mathcal{N} = \{0, 1, \ldots, N\}$. The trajectory of the UAV-RIS satisfies

$$\|\mathbf{q}_{\text{RIS}}[n+1] - \mathbf{q}_{\text{RIS}}[n]\|^2 = \frac{1}{N}\|\mathbf{q}_{\text{RIS}}[N] - \mathbf{q}_{\text{RIS}}[0]\|^2, \quad (1)$$

where $\mathbf{q}_{\text{RIS}}[0]$ and $\mathbf{q}_{\text{RIS}}[N]$ are the horizontal coordinates of the UAV-RIS's starting and ending points, respectively. In the n-th time slot, the channel between the BS and the UAV-RIS, $\mathbf{G}[n] \in \mathbb{C}^{R\times M}$, and the channel between the UAV-RIS and the k-th UE, $\mathbf{h}_k[n] \in \mathbb{C}^{R\times 1}$, $k \in \mathcal{K} = \{1, \ldots, K\}$, can be modeled as line-of-sight channels [2], [10], given respectively by

$$\mathbf{G}[n] = \sqrt{\beta d_{\text{BR}}^{-\kappa}[n]}\mathbf{a}_{\text{RIS}}(\psi[n])\mathbf{a}_{\text{BS}}^{\text{H}}(\omega[n]), \quad (2)$$

$$\mathbf{h}_k[n] = \sqrt{\beta d_{\text{RU},k}^{-\tau}[n]}\mathbf{a}_{\text{RIS}}(\nu_k[n]), \quad (3)$$

where β is the channel power gain at unit distance, κ and τ are the corresponding path loss exponents, while $d_{\text{BR}}[n] = \sqrt{H^2 + \|\mathbf{q}_{\text{RIS}}[n] - \mathbf{l}_{\text{BS}}\|^2}$ is the distance from the BS to the UAV-RIS and $d_{\text{RU},k}[n] = \sqrt{H^2 + \|\mathbf{q}_{\text{RIS}}[n] - \mathbf{l}_{\text{UE},k}\|^2}$ is the distance from the UAV-RIS to the k-th UE, with $\mathbf{l}_{\text{BS}}$ and $\mathbf{l}_{\text{UE},k}$ being the horizontal coordinates of the BS and the k-th UE, respectively. Additionally, the RIS receive array response vector and the BS transmit array response vector are given respectively by

$$\mathbf{a}_{\text{RIS}}(\psi[n]) = \big[1, \mathrm{e}^{-j\frac{2\pi d}{\lambda}(\psi_x[n]+\psi_y[n])}, \ldots, \mathrm{e}^{-j\frac{2\pi d}{\lambda}((R_x-1)\psi_x[n]+(R_y-1)\psi_y[n])}\big]^{\text{T}}, \quad (4)$$

$$\mathbf{a}_{\text{BS}}(\omega[n]) = \big[1, \mathrm{e}^{-j\frac{2\pi d}{\lambda}\omega[n]}, \ldots, \mathrm{e}^{-j\frac{2\pi d}{\lambda}(M-1)\omega[n]}\big]^{\text{T}}, \quad (5)$$

where $\psi_x[n] = \sin\big(\phi_{R_1}[n]\big)\sin\big(\phi_{R_2}[n]\big)$ and $\psi_y[n] = \cos\big(\phi_{R_1}[n]\big)\sin\big(\phi_{R_2}[n]\big)$, $\phi_{R_1}[n]$ and $\phi_{R_2}[n]$ represent the azimuth and elevation angles of arrival from the BS to the UAV-RIS in the time slot n, respectively [2], while $\omega[n]$ is the cosine of the BS's angle of departure (AoD), λ is the carrier wavelength, and d is the antenna spacing. Similarly, the RIS transmit array response vector is expressed as

$$\mathbf{a}_{\text{RIS}}(\nu_k[n]) = \big[1, \mathrm{e}^{-j\frac{2\pi d}{\lambda}(\nu_{k,x}[n]+\nu_{k,y}[n])}, \ldots, \mathrm{e}^{-j\frac{2\pi d}{\lambda}((R_x-1)\nu_{k,x}[n]+(R_y-1)\nu_{k,x}[n])}\big]^{\text{T}}, \quad (6)$$

where $\nu_{k,x}[n] = \sin\big(\phi_{U_1,k}[n]\big)\sin\big(\phi_{U_2,k}[n]\big)$ and $\nu_{k,y}[n] = \cos\big(\phi_{U_1,k}[n]\big)\sin\big(\phi_{U_2,k}[n]\big)$, $\phi_{U_1,k}[n]$ and $\phi_{U_2,k}[n]$ represent the azimuth and elevation AoDs from the UAV-RIS to the k-th UE in the time slot n, respectively. For the RIS-assisted system, the fine-grained channel information can be estimated by evaluating the path parameters using parameter-based channel reconstruction methods [11]. In the n-th time slot, the BS's complex baseband transmission signal is given by

$$\mathbf{x}[n] = \sum_{k=1}^{K}\mathbf{w}_k[n]\sqrt{p_k[n]}s_k[n], \quad (7)$$

in which $s_k[n]$ is the transmitted data for the k-th UE in the n-th time slot, $\mathbf{W}[n] = [\mathbf{w}_1[n], \ldots, \mathbf{w}_K[n]]^{\text{H}} \in \mathbb{C}^{K\times M}$ stands for the BS's active beamforming matrix, with $\mathbf{w}_k[n] \in \mathbb{C}^{M\times 1}$ and $\|\mathbf{w}_k[n]\|^2 = 1, \forall n, k$, while the BS power allocation vector is defined as $\mathbf{p}[n] = [p_1[n], \ldots, p_K[n]]^{\text{T}} \in \mathbb{C}^{K\times 1}$.

B. Problem Formulation

Let $\mathbf{\Phi}[n] = \text{diag}\{\varphi_1[n], \ldots, \varphi_R[n]\} \in \mathbb{C}^{R\times R}$ be the RIS's phase-shift matrix, where $\varphi_r[n] = e^{j\theta_r[n]}$, $\theta_r[n] \in [0, 2\pi)$ and $r \in \mathcal{R} = \{1, \ldots, R\}$. The signal-to-interference-plus-noise ratio (SINR) of the k-th UE in the n-th time slot is calculated as

$$\gamma_k[n] = \frac{\big|\mathbf{h}_k^{\text{H}}[n]\mathbf{\Phi}[n]\mathbf{G}[n]\mathbf{w}_k[n]\big|^2 p_k[n]}{\sum\limits_{i=1, i\neq k}^{K}\big|\mathbf{h}_k^{\text{H}}[n]\mathbf{\Phi}[n]\mathbf{G}[n]\mathbf{w}_i[n]\big|^2 p_i[n] + \sigma_\delta^2}, \quad (8)$$

where σ_δ^2 is the noise power. Since the optimization problem has the same mathematical expression in every time slot, the index n is dropped and the sum-rate maximization problem for all UEs per time slot is formulated as

$$\mathcal{P}(A): \max_{\mathbf{p},\mathbf{W},\mathbf{\Phi}} f_1(\mathbf{p}, \mathbf{W}, \mathbf{\Phi}) = \sum_{k=1}^{K}\varpi_k \log_2(1+\gamma_k), \quad (9a)$$

$$\text{s.t.} \sum_{k=1}^{K} p_k \leq P_{\max}, p_k > 0, \forall k, \quad (9b)$$

$$\|\mathbf{w}_k\|^2 = 1, \forall k, \quad (9c)$$

$$|\varphi_r|^2 = 1, \forall r, \quad (9d)$$

where ϖ_k is the weight for the k-th UE, constraint (9b) imposes the total transmission power limit $P_{\max}$ on the BS, constraint (9c) ensures the unit modulus for the BS's active beamforming vectors, and constraint (9d) maintains the unit modulus for the RIS's passive beamforming elements.

III. Joint Optimization

A. Equivalent Transformation of Optimization Problem

The problem $\mathcal{P}(A)$ is first equivalently transformed using the FP algorithm [7], which includes two key steps: the Lagrangian dual transformation and the quadratic transformation method. By applying the Lagrangian dual transformation, we introduce an auxiliary variable $\boldsymbol{\chi} = [\chi_1, ..., \chi_K]^{\text{T}}$. According to the quadratic transformation method, we introduce an auxiliary variable $\boldsymbol{\rho} = [\rho_1, ..., \rho_K]^{\text{T}}$. The problem $\mathcal{P}(A)$ can then be equivalently transformed into

$$\mathcal{P}(B): \max_{\mathbf{p},\mathbf{W},\mathbf{\Phi},\boldsymbol{\chi},\boldsymbol{\rho}} f_2(\mathbf{p}, \mathbf{W}, \mathbf{\Phi}, \boldsymbol{\chi}, \boldsymbol{\rho}), \text{ s.t. (9b), (9c), (9d)}, \quad (10)$$

where $f_2(\mathbf{p}, \mathbf{W}, \mathbf{\Phi}, \boldsymbol{\chi}, \boldsymbol{\rho}) = \sum_{k=1}^{K}\Big(\varpi_k \log_2(1+\chi_k) - \varpi_k\chi_k + 2\sqrt{\varpi_k(1+\chi_k)}\Re\{\rho_k^*\sqrt{p_k}\hat{\mathbf{h}}_k\mathbf{w}_k\} - |\rho_k|^2\big(\sum_{i=1}^{K} p_i|\hat{\mathbf{h}}_k\mathbf{w}_i|^2 + \sigma_\delta^2\big)\Big)$, and $\hat{\mathbf{h}}_k = \mathbf{h}_k^{\text{H}}\mathbf{\Phi}\mathbf{G}$.

Given the optimization variables $\mathbf{p}$, $\mathbf{W}$ and $\mathbf{\Phi}$, the optimal χ_k and ρ_k can be expressed as

$$\tilde{\chi}_k = \gamma_k, \ \tilde{\rho}_k = \frac{\sqrt{\varpi_k(1+\chi_k)p_k}\hat{\mathbf{h}}_k\mathbf{w}_k}{\sum\limits_{i=1}^{K} p_i\big|\hat{\mathbf{h}}_k\mathbf{w}_i\big|^2 + \sigma_\delta^2}. \quad (11)$$

B. Optimization of BS Power Allocation

Given the optimization variables $\mathbf{W}$ and $\mathbf{\Phi}$, the problem $\mathcal{P}(B)$ becomes

$$\mathcal{P}(C): \max_{\mathbf{p},\boldsymbol{\chi},\boldsymbol{\rho}} f_2(\mathbf{p}, \boldsymbol{\chi}, \boldsymbol{\rho}), \text{ s.t. (9b)}. \quad (12)$$

We solve $\mathcal{P}(C)$ by applying the AO algorithm to alternately optimize the variables $\mathbf{p}$, $\boldsymbol{\chi}$ and $\boldsymbol{\rho}$ until the value of $f_2(\mathbf{p},\boldsymbol{\chi},\boldsymbol{\rho})$ converges. Specifically, given $\mathbf{p}$, $\boldsymbol{\chi}$ and $\boldsymbol{\rho}$ are updated by (11). Given $\boldsymbol{\chi}$ and $\boldsymbol{\rho}$, the problem $\mathcal{P}(C)$ becomes a convex optimization problem with respect to $\mathbf{p}$. The convexity of $\mathcal{P}(C)$ allows us to apply the Karush-Kuhn-Tucker conditions to directly solve for the optimal solution p_k, yielding

$$\tilde{p}_k = \left(\frac{\sqrt{\varpi_k(1+\chi_k)}\Re\{\rho_k^*\hat{\mathbf{h}}_k\mathbf{w}_k\}}{\sum_{i=1}^K(|\rho_i|^2|\hat{\mathbf{h}}_i\mathbf{w}_k|^2)+Lr} \right)^2, \tag{13}$$

where Lr is the Lagrange multiplier for the power constraint (9b), which can be obtained by the bisection method [10].

C. Optimization of Active and Passive Beamforming

Given the optimization variable $\mathbf{p}$, $\mathcal{P}(B)$ becomes

$$\mathcal{P}(D): \max_{\mathbf{W},\boldsymbol{\Phi},\boldsymbol{\chi},\boldsymbol{\rho}} f_2(\mathbf{W},\boldsymbol{\Phi},\boldsymbol{\chi},\boldsymbol{\rho}), \text{ s.t. (9c), (9d).} \tag{14}$$

We apply the AO algorithm to solve $\mathcal{P}(D)$ by alternately optimizing $\mathbf{W}$, $\boldsymbol{\Phi}$, $\boldsymbol{\chi}$ and $\boldsymbol{\rho}$ until the value $f_2(\mathbf{W},\boldsymbol{\Phi},\boldsymbol{\chi},\boldsymbol{\rho})$ converges. First recall that given $\mathbf{W}$ and $\boldsymbol{\Phi}$, the variables $\boldsymbol{\chi}$ and $\boldsymbol{\rho}$ are updated by (11).

Given $\boldsymbol{\Phi}$, $\boldsymbol{\chi}$ and $\boldsymbol{\rho}$, we proceed to optimize the variable $\mathbf{W}$. To facilitate this optimization, the constraint (9c) is transformed into a standard Riemannian manifold, i.e., $\mathbf{I}_{K\times K}\circ\big(\mathbf{W}\mathbf{W}^{\mathrm{H}}\big)=\mathbf{I}_{K\times K}$, where $\mathbf{I}_{K\times K}$ denotes the $K\times K$ identity matrix and $\circ$ represents element-wise multiplication [9]. Then the problem $\mathcal{P}(D)$ is reformulated as

$$\max_{\mathbf{W}} f_2(\mathbf{W}), \text{ s.t. } \mathbf{I}_{K\times K}\circ\big(\mathbf{W}\mathbf{W}^{\mathrm{H}}\big)=\mathbf{I}_{K\times K}. \tag{15}$$

The constraint set for $\mathbf{W}$ defines an Oblique manifold, denoted as $\mathcal{A}$, which is characterized as

$$\mathcal{A}=\big\{\mathbf{W}\in\mathbb{C}^{K\times M}:\mathbf{I}_{K\times K}\circ\big(\mathbf{W}\mathbf{W}^{\mathrm{H}}\big)=\mathbf{I}_{K\times K}\big\}. \tag{16}$$

We apply the Oblique conjugate gradient algorithm [9] to obtain the steady-state solution of $f_2(\mathbf{W})$, which utilizes the Polak-Ribiére conjugate gradient direction for search direction. The j-th Oblique manifold iteration is detailed as follows.

1) Calculation of Oblique gradient:

$$\mathrm{grad}f_{\mathcal{A}}\big(\mathbf{W}^{(j)}\big)=\nabla f_2\big(\mathbf{W}^{(j)}\big) - \big(\mathbf{I}_{K\times K}\circ\Re\big\{\mathbf{W}^{(j)}(\nabla f_2(\mathbf{W}^{(j)}))^{\mathrm{H}}\big\}\big)\mathbf{W}^{(j)}, \tag{17}$$

where $\nabla f_2(\mathbf{W}^{(j)})$ is the Euclidean gradient of $f_2(\mathbf{W}^{(j)})$, given by

$$\nabla f_2(\mathbf{W}^{(j)})=\begin{bmatrix} \sqrt{\varpi_1(1+\chi_1)p_1}\rho_1^*\hat{\mathbf{h}}_1-\sum_{k=1}^K|\rho_k|^2p_1\mathbf{w}_1^{\mathrm{H}}\hat{\mathbf{h}}_k^{\mathrm{H}}\hat{\mathbf{h}}_k \\ \vdots \\ \sqrt{\varpi_K(1+\chi_K)p_K}\rho_K^*\hat{\mathbf{h}}_K-\sum_{k=1}^K|\rho_k|^2p_K\mathbf{w}_K^{\mathrm{H}}\hat{\mathbf{h}}_k^{\mathrm{H}}\hat{\mathbf{h}}_k \end{bmatrix}. \tag{18}$$

2) Determine the search direction $\mathbf{d}_{\mathcal{A}}^{(j)}$:

$$\mathbf{d}_{\mathcal{A}}^{(j)}=-\mathrm{grad}f_{\mathcal{A}}\big(\mathbf{W}^{(j)}\big)+\beta_{\mathcal{A}}^{(j)}\mathcal{T}_{\mathcal{A}}\big(\mathbf{d}_{\mathcal{A}}^{(j-1)}\big), \tag{19}$$

where $\beta_{\mathcal{A}}^{(j)}$ is the Polak-Ribiére conjugate gradient update parameter and $\mathcal{T}_{\mathcal{A}}(\mathbf{d}_{\mathcal{A}}^{(j-1)})$ stands for the projection function on the Oblique manifold, given respectively by

$$\beta_{\mathcal{A}}^{(j)}=\frac{\nabla f_2^{\mathrm{H}}(\mathbf{W}^{(j)})\big(\nabla f_2(\mathbf{W}^{(j)})-\mathcal{T}_{\mathcal{A}}(\nabla f_2(\mathbf{W}^{(j-1)}))\big)}{\|\nabla f_2(\mathbf{W}^{(j-1)})\|^2}, \tag{20}$$

$$\mathcal{T}_{\mathcal{A}}\big(\mathbf{d}_{\mathcal{A}}^{(j-1)}\big)=\mathbf{d}_{\mathcal{A}}^{(j-1)}-\big(\mathbf{I}_{K\times K}\circ\Re\big\{\mathbf{W}^{(j)}(\mathbf{d}_{\mathcal{A}}^{(j-1)})^{\mathrm{H}}\big\}\big)\mathbf{W}^{(j)}. \tag{21}$$

3) Employ the Armijo backtracking line search algorithm to select the step size u_1, update $\mathbf{W}^{(j+1)}$, and retract back onto Oblique manifold:

$$\mathbf{W}^{(j+1)}=\begin{bmatrix} \frac{w_{11}^{(j)}+u_1d_{\mathcal{A},11}^{(j)}}{\sqrt{\sum_{i=1}^K|w_{i1}^{(j)}+u_1d_{\mathcal{A},i1}^{(j)}|^2}} & \cdots & \frac{w_{1M}^{(j)}+u_1d_{\mathcal{A},1M}^{(j)}}{\sqrt{\sum_{i=1}^K|w_{iM}^{(j)}+u_1d_{\mathcal{A},iM}^{(j)}|^2}} \\ \vdots & \ddots & \vdots \\ \frac{w_{K1}^{(j)}+u_1d_{\mathcal{A},K1}^{(j)}}{\sqrt{\sum_{i=1}^K|w_{i1}^{(j)}+u_1d_{\mathcal{A},i1}^{(j)}|^2}} & \cdots & \frac{w_{KM}^{(j)}+u_1d_{\mathcal{A},KM}^{(j)}}{\sqrt{\sum_{i=1}^K|w_{iM}^{(j)}+u_1d_{\mathcal{A},iM}^{(j)}|^2}} \end{bmatrix}, \tag{22}$$

where w_{km} and $d_{\mathcal{A},km}^{(j)}$ are the k-th row and m-th column elements of $\mathbf{W}$ and $\mathbf{d}_{\mathcal{A}}^{(j)}$, respectively.

Given $\mathbf{W}$, $\boldsymbol{\chi}$ and $\boldsymbol{\rho}$, we proceed to optimize the variable $\boldsymbol{\Phi}$. Let $\hat{\mathbf{h}}_k\mathbf{w}_k=\boldsymbol{\varphi}^{\mathrm{H}}\mathrm{diag}\big\{\mathbf{h}_k^{\mathrm{H}}\big\}\mathbf{G}\mathbf{w}_k=\boldsymbol{\varphi}^{\mathrm{H}}\mathbf{z}_{k,k}$, where $\boldsymbol{\varphi}=\big[\varphi_1,\ldots,\varphi_R\big]^{\mathrm{H}}$ and $\mathbf{z}_{k,i}=\mathrm{diag}\big\{\mathbf{h}_k^{\mathrm{H}}\big\}\mathbf{G}\mathbf{w}_i$. Then the problem $\mathcal{P}(D)$ can be reformulated as

$$\min_{\boldsymbol{\varphi}} f_3(\boldsymbol{\varphi})=\boldsymbol{\varphi}^{\mathrm{H}}\mathbf{A}\boldsymbol{\varphi}-2\Re\big\{\boldsymbol{\varphi}^{\mathrm{H}}\mathbf{b}\big\}, \text{ s.t. (9d),} \tag{23}$$

where $\mathbf{A}=\sum_{k=1}^K\big(|\rho_k|^2\sum_{i=1}^K\mathbf{z}_{k,i}\mathbf{z}_{k,i}^{\mathrm{H}}p_i\big)\in\mathbb{C}^{R\times R}$ and $\mathbf{b}=\sum_{k=1}^K\sqrt{\varpi_k(1+\chi_k)p_k}\rho_k^*\mathbf{z}_{k,k}\in\mathbb{C}^{R\times 1}$. The constraint set for $\boldsymbol{\varphi}$ defines a Riemannian manifold C which is given by

$$C=\big\{\boldsymbol{\varphi}\in\mathbb{C}^{R\times 1}:|\varphi_r|^2=1,r=1,\ldots,R\big\}. \tag{24}$$

We employ the Riemannian conjugate gradient algorithm to obtain the steady-state solution of $f_3(\boldsymbol{\varphi})$, which utilizes the Polak-Ribiére conjugate gradient direction for search direction. The j-th Riemannian manifold iteration can be written as

1) Calculation of Riemannian gradient:

$$\mathrm{grad}f_C(\boldsymbol{\varphi}^{(j)})=\nabla f_3(\boldsymbol{\varphi}^{(j)})-\Re\{\nabla f_3(\boldsymbol{\varphi}^{(j)})\circ(\boldsymbol{\varphi}^{(j)})^*\}\circ\boldsymbol{\varphi}^{(j)}, \tag{25}$$

where $\nabla f_3(\boldsymbol{\varphi}^{(j)})$ is the Euclidean gradient of $f_3(\boldsymbol{\varphi}^{(j)})$, given by

$$\nabla f_3(\boldsymbol{\varphi}^{(j)})=\mathbf{A}\boldsymbol{\varphi}-\mathbf{b}. \tag{26}$$

2) Determine the search direction $\mathbf{d}_C^{(j)}$:

$$\mathbf{d}_C^{(j)}=-\mathrm{grad}f_C(\boldsymbol{\varphi}^{(j)})+\beta_C^{(j)}\mathcal{T}_C\big(\mathbf{d}_C^{(j-1)}\big), \tag{27}$$

where $\beta_C^{(j)}$ has the same form as $\beta_{\mathcal{A}}^{(j)}$ in (20), and $\mathcal{T}_C\big(\mathbf{d}_C^{(j-1)}\big)$ is the projection function on the Riemannian manifold

$$\mathcal{T}_C\big(\mathbf{d}_C^{(j-1)}\big)=\mathbf{d}_C^{(j-1)}-\Re\big\{\mathbf{d}_C^{(j-1)}\circ(\boldsymbol{\varphi}^{(j)})^*\big\}\circ\boldsymbol{\varphi}^{(j)}. \tag{28}$$

3) Employ the Armijo backtracking line search algorithm to select the step size u_2, update $\boldsymbol{\varphi}^{(j+1)}$, and retract back onto Oblique manifold:

$$\boldsymbol{\varphi}^{(j+1)}=\left[\frac{\varphi_1+u_2d_{C,1}^{(j)}}{|\varphi_1+u_2d_{C,1}^{(j)}|},\ldots,\frac{\varphi_R+u_2d_{C,R}^{(j)}}{|\varphi_R+u_2d_{C,R}^{(j)}|}\right]^{\mathrm{T}}. \tag{29}$$

D. Algorithm Analysis

The joint optimization of $\mathbf{p}$, $\mathbf{W}$ and $\boldsymbol{\Phi}$ is listed in Algorithm 1. The BS power allocation algorithm has the complexity of $\mathcal{O}\big(I_{Lr}I_1K^3\big)$, where I_{Lr} and I_1 are the numbers of iterations for bisection search of Lr and for within the phase search, respectively. The complexity of the active and passive beamforming joint optimization algorithm using FP-manifold mainly depends on the computation of the conjugate

Algorithm 1 Proposed PBCD algorithm framework.

Initialize $\mathbf{p}^{(0)}$, $\mathbf{W}^{(0)}$ and $\mathbf{\Phi}^{(0)}$, Set $t_1 = t_2 = t_3 = 0$;
repeat
  $t_1 = t_1 + 1$;
  repeat
    $t_2 = t_2 + 1$;
    Update variables $\boldsymbol{\chi}^{(t_2)}$ and $\boldsymbol{\rho}^{(t_2)}$ by (11);
    Update power allocation vector $\mathbf{p}^{(t_2)}$ by (13);
  until $\mathcal{P}(C)$ converges.
  repeat
    $t_3 = t_3 + 1$;
    Update variables $\boldsymbol{\chi}^{(t_3)}$ and $\boldsymbol{\rho}^{(t_3)}$ by (11);
    Update active beamforming $\mathbf{W}^{(t_3)}$ by (22);
    Update passive beamforming $\boldsymbol{\varphi}^{(t_3)}$ by (29);
  until $\mathcal{P}(D)$ converges.
  $\mathbf{p}^{(t_1)} = \mathbf{p}^{(t_2)}$, $\mathbf{\Phi}^{(t_1)} = \mathrm{diag}\{\boldsymbol{\varphi}^{(t_3)}\}$, $\mathbf{W}^{(t_1)} = \mathbf{W}^{(t_3)}$;
until $\mathcal{P}(A)$ converges.

gradients. According to (18) and (26), the complexity of computing the gradients are $\mathcal{O}(K^2M)$ and $\mathcal{O}(K^2R)$, respectively. Thus, the total complexity of the proposed algorithm is $\mathcal{O}\big(I_O(I_{Lr}I_1K^3+I_2(I_WK^2M+I_\Phi K^2R))\big)$, where I_W and I_Φ are the numbers of iterations for the Oblique manifold and Riemannian manifold conjugate gradient algorithms, while I_2 and I_O are the numbers of iterations within and between phases, respectively. The complexity comparison with the baseline schemes is shown in Table I. Our PBCD algorithm framework decomposes the optimization problem into phases based on the underlying characteristics of the variables, enabling more efficient optimization. This results in a lower number of required iterations (I_O) compared to the baselines (I_{O1} and I_{O2}). As a result, the proposed algorithm achieves lower computational complexity, especially when $R \gg K$.

IV. Simulations

We carry out extensive simulations to demonstrate the superiority of our proposed PBCD algorithm framework, including our BS power allocation optimization algorithm based on FP and our joint optimization algorithm for active and passive beamforming based on FP manifold optimization.

According to the UAV-RIS flight trajectory L and flight speed $V_{\text{avg}} = 8.5\,\text{m/s}$, the flight cycle is partitioned into 21 equal time slots. Each time slot corresponds to an equivalent position (EP) point, with each time slot having a duration of $\nabla t = 1\,\text{s}$. The EP points corresponding to the 21 time slots, starting at $\mathbf{q}_{\text{RIS}}[0]$ and ending at $\mathbf{q}_{\text{RIS}}[N]$ on the flight trajectory L, are shown in Fig. 2. $\mathbf{q}_{\text{RIS}}[0] = [-10, 110]\,\text{m}$, $\mathbf{q}_{\text{RIS}}[N] = [110, -10]\,\text{m}$ and the BS coordinates are set as $\mathbf{l}_{\text{BS}} = [0, 100]\,\text{m}$. The system supports $K = 4$ UEs, which are

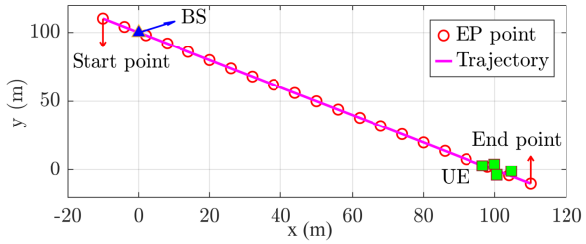

Fig. 2. The diagram of BS, UE coordinates and UAV-RIS trajectory.

uniformly and randomly distributed within a circle centered at $(100\,\text{m}, 0\,\text{m})$ with a radius of $10\,\text{m}$. The distance between the BS and the UE regional center is $d_{\text{BU}} = 141\,\text{m}$. The path loss exponents κ and τ are both set to 2, the unit distance channel gain is set as $\beta = 30\,\text{dB}$, while the noise power spectral density is $-170\,\text{dBm/Hz}$. Other default simulation system's parameters are as follows: the UAV-RIS height $H = 40\,\text{m}$, the maximum BS transmitting power $P_{\text{max}} = 40\,\text{dBm}$, the number of RIS units $R = 100$, and the number of the BS antennas $M = 50$. Assuming that the UAV-RIS is located at the 11-th EP point $\mathbf{q}_{\text{RIS}}[10]$, counting from the starting point $\mathbf{q}_{\text{RIS}}[0]$.

The schemes compared in the simulation are listed in Table II, and they are further explained as follows.

- PBCD+FP_manifold[1], BCD+FP_manifold and AO+FP_manifold: For these three schemes, the algorithmic frameworks employed are the proposed PBCD, the existing BCD and AO, respectively. The power allocation is designed based on the FP algorithm, while the active and passive beamforming with unit mode constraints are designed using the proposed FP-Manifold algorithm.
- PBCD+SCA and BCD+SCA [7]: These two schemes utilize the proposed PBCD and the existing BCD as the algorithmic frameworks, respectively. The active beamforming without unit mode constraints is designed using standard convex optimization, and the passive beamforming is designed using the existing SCA algorithm.
- PBCD+Manifold and AO+Manifold [9]: For these two schemes, the algorithmic frameworks employed are the proposed PBCD and the existing AO, respectively. The power allocation is designed using the existing GP, while the active and passive beamforming with unit mode constraints are designed using the existing manifold algorithms.

We also test a scheme called Random $\mathbf{\Phi}$, which chooses the elements of $\mathbf{\Phi}$ randomly in the range $[0, 2\pi)$, and designs other variables using the algorithm proposed in this paper.

[1]We adopt the A+B naming rule, where component A indicates the principal algorithmic framework and component B specifies the critical variable optimization technique that predominantly determines the overall computational complexity.

TABLE II
Explanation of Different Schemes in Simulation

Framework and Algorithm \ Scheme	PBCD+FP_manifold (in this paper)	BCD+ FP_manifold	AO+ FP_manifold	PBCD+SCA	BCD+ SCA [7]	PBCD+ Manifold	AO+Manifold [9]
Framework	PBCD	BCD	AO	PBCD	BCD	PBCD	AO
Algorithm for Optimization $\mathbf{p}$	FP	FP	FP	Convex (Jointly)	Convex (Jointly)	GP	GP
Algorithm for Optimization $\mathbf{W}$	FP-manifold (Jointly)	FP-manifold	FP-manifold			Manifold (Jointly)	Manifold
Algorithm for Optimization $\mathbf{\Phi}$		FP-manifold	FP-manifold	SCA	SCA		Manifold

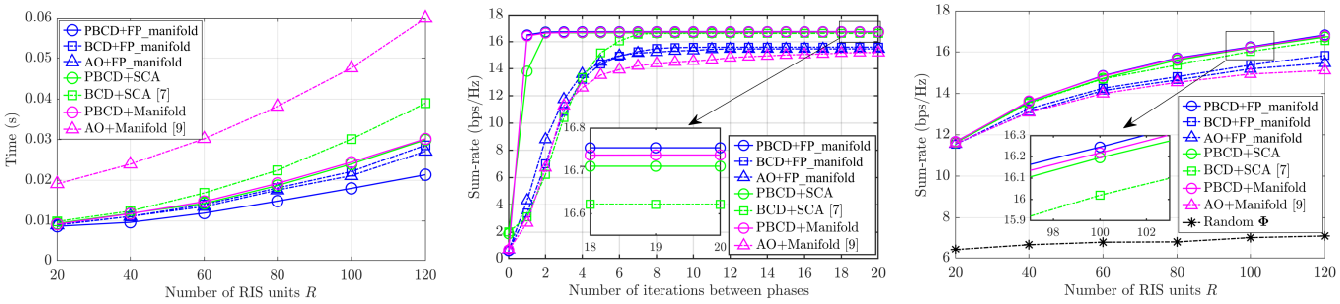

(a) (b) (c)

Fig. 3. (a) Convergence time versus number of RIS units, (b) Convergence performance versus number of iterations between phases, and (c) Sum-rate versus number of RIS units, for different algorithms.

TABLE I
COMPLEXITY COMPARISON

Scheme	Complexity
This paper	$\mathcal{O}\big(I_O(I_{Lr}I_1K^3+I_2(I_WK^2M+I_\Phi K^2R))\big)$
[7]	$\mathcal{O}(I_{O1}(2KRM+KM^2+K^2R^2))$
[9]	$\mathcal{O}(I_{O2}(K^3+K^2M^2+K^2RM))$

The convergence times of the schemes are compared using MATLAB 2020b on an Intel i5-12400F CPU with a 2.5GHz clock speed, as illustrated in Fig. 3 (a). It shows that the schemes adopting the optimization algorithms of this paper (FP_manifold) achieve shorter computation times to convergence than the other schemes. Also with the same optimization algorithms, the schemes employing our PBCD framework have lower computation times than the corresponding schemes utilizing the existing BCD and AO frameworks, and the scheme proposed in this paper (PBCD+FP_manifold) achieves the lowest computation time. This demonstrates the computational efficiency of our PBCD framework and the proposed optimization algorithms for the optimization of power allocation, active and passive beamforming. Similarly, it can be observed from Fig. 3 (b) that the PBCD framework outperforms the BCD and AO frameworks in both rate and convergence performance. Fig. 3 (c) also shows that the schemes adopting the PBCD framework have higher sum performance than the corresponding schemes adopting the BCD and AO frameworks. It can also be seen from Fig. 3 (c) that without optimizing the passive beamforming of RIS, the sum rate performance degrades dramatically.

Fig. 4 depicts the system sum-rate versus the UAV-RIS EP point and height. It can be seen that the sum rate varies with the UAV-RIS's location, exhibiting extreme values. For UAV-RIS flying above 70.5 m (i.e., $H > d_{\text{BU}}/2$), the optimal EP point is near to the midpoint between the BS and the UE. For UAV-RIS flying below 70.5 m (i.e., $H < d_{\text{BU}}/2$), the optimal EP point is closer to either the BS or UE side [12].

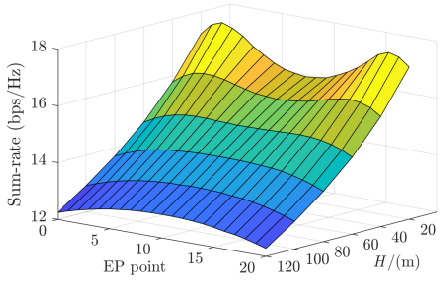

Fig. 4. Sum-rate versus UAV-RIS EP position and height achieved by the proposed PBCD+FP_manifold.

V. CONCLUSIONS

This paper has proposed a PBCD algorithm framework to maximize the system sum-rate by dividing the joint optimization into two phases: BS power allocation, and active and passive beamforming. We have presented a power allocation algorithm using the FP approach and an AO algorithm for joint active and passive beamforming based on the FP-manifold. Our PBCD algorithm framework demonstrates superiority over other algorithm frameworks in terms of convergence speed and sum-rate performance. In the joint optimization phase of active and passive beamforming, our FP-manifold-based algorithm also outperforms traditional manifold optimization algorithms in both convergence time and system sum-rate.

REFERENCES

[1] Y. Liu, *et al.*, "Reconfigurable intelligent surfaces: Principles and opportunities," *IEEE Commun. Surveys Tuts.*, vol. 23, no. 3, pp. 1546–1577, 3th Quart. 2021.

[2] X. Liu, *et al.*, "Throughput maximization for RIS-UAV relaying communications," *IEEE Trans. Intell. Transp. Syst.*, vol. 23, no. 10, pp. 19569–19574, Oct. 2022.

[3] B. Yang, *et al.*, "Performance, fairness, and tradeoff in UAV swarm underlaid mmWave cellular networks with directional antennas," *IEEE Trans. Wireless Commun.*, vol. 20, no. 4, pp. 2383–2397, Apr. 2021.

[4] M. Li, *et al.*, "Energy-efficient covert communication with the aid of aerial reconfigurable intelligent surface," *IEEE Commun. Lett.*, vol. 26, no. 9, pp. 2101–2105, Sep. 2022.

[5] Q. Wu and R. Zhang, "Intelligent reflecting surface enhanced wireless network via joint active and passive beamforming," *IEEE Trans. Wireless Commun.*, vol. 18, no. 11, pp. 5394–5409, Nov. 2019.

[6] M. A. ElMossallamy, *et al.*, "RIS optimization on the complex circle manifold for interference mitigation in interference channels," *IEEE Trans. Veh. Technol.*, vol. 70, no. 6, pp. 6184–6189, Jun. 2021.

[7] H. Guo, *et al.*, "Weighted sum-rate maximization for reconfigurable intelligent surface aided wireless networks," *IEEE Trans. Wireless Commun.*, vol. 19, no. 5, pp. 3064–3076, May 2020.

[8] X. Gu, *et al.*, "ARIS-empowered wireless communications: Joint beamforming design and deployment optimization," *IEEE Wireless Commun. Lett.*, vol. 12, no. 12, pp. 2003–2007, Dec. 2023.

[9] Y. Xiu, *et al.*, "IRS-assisted millimeter wave communications: Joint power allocation and beamforming design," in *Proc. WCNCW* (Nanjing, China), Mar. 29, 2021, pp. 1–6.

[10] Y. Cao, *et al.*, "Intelligent reflecting surface aided multi-user mmWave communications for coverage enhancement," in *Proc. PIMRC* (London, UK), Aug. 31, 2020, pp. 1–6.

[11] Y. Byun, *et al.*, "Channel estimation and phase shift control for UAV-carried RIS communication systems" *IEEE Trans. Veh. Technol.*, vol. 72, no. 10, pp. 13695–13700, Oct. 2023.

[12] A. L. Moustakas, *et al.*, "Reconfigurable intelligent surfaces and capacity optimization: A large system analysis," *IEEE Trans. Wireless Commun.*, vol. 22, no. 12, pp. 8736–8750, Dec. 2023.